ACS central science

Research Article

Cite This: ACS Cent. Sci. 2019, 5, 1017−1023

http://pubs.acs.org/journal/acscii

Spontaneous Formation of CdSe Photoluminescent Nanotubes with Visible-Light Photocatalytic Performance

Xiaopeng Huang, Virendra K. Parashar, and Martin A. M. Gijs*

Laboratory of Microsystems, Ecole Polytechnique Fédérale de Lausanne (EPFL), CH-1015 Lausanne, Switzerland

Supporting Information

ABSTRACT: Two-dimensional (2D) colloidal CdSe nanocrystals (NCs) with precise atomic-scale thickness have attracted intensive attention in recent years due to their optical properties and quantum confinement effects originating from their particular band structure. Here, we report a solution-based and template-free protocol to synthesize CdSe nanotubes (NTs) having 3−6 walls, each of which has 3.5 molecular monolayers. Their crystal structure is zincblende, with Cd-terminated {100} planes at the top and bottom surfaces of each wall, which are passivated by short-chain acetate ligands. After verifying the prominent role of the acetate ligand for NT synthesis, we elucidated the formation mechanism of these NTs. It starts by heterogeneous nucleation of 2D plateletlike nanoseeds from the amorphous Cd precursor matrix, followed by the growth via lateral and angular attachment of nanoplatelet building blocks into curved nanosheets, eventually resulting in NTs with sharp absorption and photoluminescence peak at around 460 nm. Moreover, the NTs show remarkable visible-light photocatalytic activity, as demonstrated by the reduction of the reddish Rhodamine B into its leuco form with a conversion rate of 92% in 1 min.

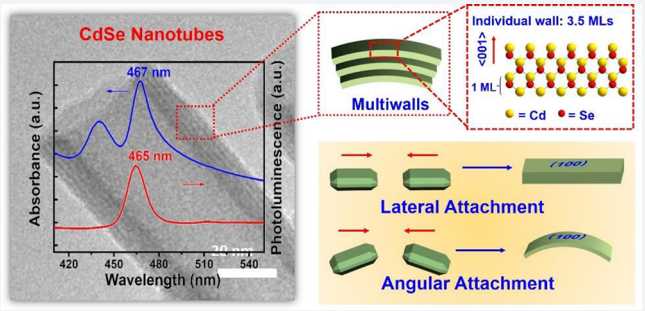

INTRODUCTION

Control over the size and shape of semiconductors at the nanoscale has resulted in materials with unique and on-demand electronic and optical properties because of quantum confinement effects.[1,2] Cadmium selenide (CdSe), the most studied II−VI group semiconductor, has been synthesized into two-dimensional (2D) free-standing colloidal nanocrystals (NCs), such as nanoribbons,[3] nanoplatelets,[4,5] nanodisks,[6] nanosheets,[7] nanobelts,[8] and nanoscrolls.[9,10] In these nanostructures, only one dimension is smaller than the excitonic Bohr radius, leading to discrete absorption and emission spectra that can be well-explained by a one-dimensional (1D) infinite potential quantum well model.[4,11−14] Despite the successful synthesis of various 2D CdSe NCs, the underlying formation mechanism remains controversial. B. Dubertret et al. first synthesized zincblende CdSe nanoplatelets in 2008 and proposed a mechanism involving two steps: producing nanoseeds with fixed thickness and subsequent lateral extension via monomer feeding.[15] D. Norris et al. further elucidated the anisotropic growth mechanism based on the 2D nucleation and growth theory and showed that enhanced growth on narrow surface facets was energetically favored in island-nucleation-limited reactions.[16] In other work, X. Peng et al. suggested that the lateral extension is by oriented attachment rather than by monomer addition.[17] Unfortunately, although they observed the building blocks, named 2D embryos, evidence on the side-selective attachment of 2D embryos to form nanoplates seems deficient. It is obvious that a much more in-depth understanding of the formation of 2D zincblende CdSe NCs is needed.

A nanotube (NT) has been an appealing nanoscale object since the discovery of carbon NTs in 1991 and can be envisioned as a seamless roll-up of a 2D nanosheet.[18,19] However, due to the hollow interior, most CdSe NTs synthesis so far required the usage of sacrificial templates, like ZnO nanorods or $Cd(OH)_2$ nanowires.[20,21] Uniform and ultrathin tube walls are difficult to achieve by these approaches. Considering the high symmetry of the zincblende structure, synthesis of CdSe nanotubes with atomically flat walls is of great technical difficulty. In this study, we disclose a template-free protocol to synthesize colloidal CdSe NTs evolved from 2D CdSe nanoplatelets and nanosheets. An individual tube is identified to have 3−6 walls, each of which consists of 3.5 molecular monolayers (MLs) in thickness. The NTs have a zincblende structure, with both top and bottom surfaces of each wall terminated by Cd {100} planes. We studied their properties and elucidated their formation mechanism by scanning electron microscopy (SEM), transmission electron microscopy (TEM), high-resolution TEM (HRTEM), high-angle annular dark-field scanning transmission electron microscopy (HAADF-STEM), selected-area electron diffraction (SAED), X-ray diffraction (XRD), and ultraviolet−visible

Received: February 23, 2019
Published: May 2, 2019

DOI: 10.1021/acscentsci.9b00184
ACS Cent. Sci. 2019, 5, 1017−1023

(UV−vis) absorption and photoluminescence (PL) spectroscopies.

RESULTS AND DISCUSSION

Morphology and Crystal Structure of CdSe NTs. A typical synthetic protocol of CdSe NTs starts with preparing clear Cd precursor solutions by dissolving cadmium acetate dihydrate ($Cd(Ac)_2{\cdot}2H_2O$) powder in dioctyl amine (DOA) at 200 °C, which we label as "$Cd(Ac)_2$-DOA Solution". The latter was rapidly injected into a hot 1-octadecene (ODE) solution containing Se powder at 260 °C (Figure S1a). White microparticles immediately precipitated and gradually turned into yellow and brown products during the reaction. A reaction time of 8 min gave well-defined bundles of CdSe NTs with a hollow interior, as shown in the SEM graph of Figure 1a. Since

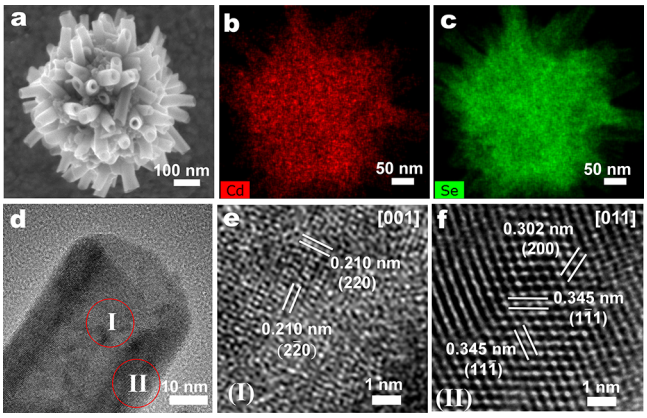

Figure 1. Structural and elemental characterization of CdSe nanotubes (NTs) by scanning electron microscopy (SEM) and high-resolution transmission electron microscopy (HRTEM). (a) SEM graph of a bundle of CdSe NTs, with elemental mapping of (b) Cd and (c) Se. (d) HRTEM graph of a CdSe NT, with (e, f) close-ups of the center (e, part I in d), showing 0.210 nm lattice spacing corresponding to the {220} planes of the CdSe zincblende structure, and the edge (f, part II in d), showing 0.302 and 0.345 nm lattice spacings corresponding to the {200} and {111} planes, respectively, indicating that the growth direction along the thickness of the NT is ⟨100⟩.

no long-chain strong ligands, such as oleic acid or trioctyl phosphine oxide, were used in the process, which are known to result in stable individual quantum dots or nanoplatelets,[22,23] NTs formed aggregates of several hundred nanometers. The energy-dispersive X-ray spectra (EDX) mapping shows the presence of both Cd and Se elements over the whole nanostructure (Figure 1b,c). Our semiquantitative analysis demonstrates the excess of Cd over Se with a ratio of 1.5:1 between Cd and Se atoms (Figure S2). The tubular architecture is also evident from (1) the sharp contrast between the center and edge of the tube as visualized using STEM (Figure S1e), (2) an intact ring-shape opening of the tube visible in TEM (Figure S1f), and (3) an enlargement of the tube opening after tilting the TEM sample rod at an angle of 25° (Figure S1g,h). On the basis of these microscopic observations, the diameter and length of a tube are estimated to be in the range 25−50 and 60−200 nm, respectively.

In classical synthetic protocols, 2D CdSe NCs with a zincblende structure were obtained using both short-chain and long-chain $Cd(carboxylate)_2$ as precursors, while amine-containing solvent was mainly employed for those with wurtzite structure.[11−14] Despite the addition of DOA in our protocol, the crystal structure of our NTs was proven to be zincblende, as characterized by XRD and SAED (Figure S3). We then determined the crystallographic orientation on the tube using HRTEM. In the center of the NT (region I in Figure 1d), characteristic fringe spacings of 0.210 nm indicate the presence of two orthogonal {220} planes viewed along the ⟨001⟩ direction (Figure 1e), consistent with a fast Fourier transform (FFT) pattern presenting 4-fold rotational symmetry (Figure S4b). This suggests that both the lateral and angular growth directions on the surface of the NT are parallel to the ⟨110⟩ direction, while the thickness direction is parallel to the ⟨001⟩ direction. We further confirmed this by the observations on the edge of an NT (region II in Figure 1d), which presented characteristic fringe spacings of 0.345, 0.345, and 0.302 nm, corresponding to two {111} planes and one {200} plane in zincblende CdSe, respectively (Figure 1f); the corresponding zone axis is in the ⟨110⟩ direction (Figure S4c). Similar results can be found upon observation along the opening of an NT (Figure S4d,e).

For CdSe NTs synthesized within 8 min, the measured wall thickness is 6∼12 nm. The NT of Figure 2a has a wall thickness of 10 nm, as determined by TEM, with some discernible stripes suggesting that it might consist of substructures. The NTs optical spectra indicate an ensemble of 2D CdSe NCs with a uniform thickness of 3.5 MLs[10] (Figure 2d). Two sharp peaks at 467 and 440 nm in the UV−vis absorption spectra are attributed to heavy-hole and light-hole transition in 2D CdSe NCs.[4] The sharp PL peak at 465 nm with a full width at half-maximum (fwhm) of 13 nm further validates the 1D quantum confinement. The anti-Stokes red-shift of 2 nm in the absorption spectra could arise from strong interwall coupling inside the nanostructures[7] and scattering within the sample. The latter is deduced by comparison with the PL-excitation spectra, showing no scattering signal and no anti-Stokes shift (Figure S5). We thus hypothesize that these NTs are composed of 3−6 walls, each having a thickness of 3.5 MLs (Figure 2j). Moreover, both top and bottom surfaces of a wall are terminated with Cd atoms capped with acetate ligand along the ⟨001⟩ direction (Figure 2l), a configuration that results from the balance of van der Waals (VdW) attraction[24] and dipole−dipole repulsion[25] between adjacent walls.

We obtained evidence to support this hypothesis by directly observing the NTs with high-magnification STEM, which display multiple linear features with good contrast (Figure 2g). When observed along the opening of an NT, the closure of NTs on an individual-wall scale can be observed, from which we deduce an interwall spacing of less than 1 nm (Figure 2h,i). By comparing the STEM and TEM graphs of the same NTs, we find that the NTs synthesized within 8 min are highly sensitive to the electron beam used under high-magnification TEM (Figure S6), which would eventually lead to blurred images. We thus performed Fourier transform infrared spectroscopy (FTIR) to discern the capping ligand existing on the NTs. As shown in Figure S7, the peaks at 1538 and 1408 cm^{-1}, corresponding to the asymmetric and symmetric stretching vibrations of COO− on acetate, are much stronger than the peaks at 2922 and 2852 cm^{-1} that represent the stretching vibrations of C−H on DOA. This confirms that acetate rather than DOA plays the leading role in capping the CdSe NTs synthesized within 8 min. Assuming the walls are attracted to each other by VdW interaction, we envisaged that individual walls could be differentiated by substituting acetate

DOI: 10.1021/acscentsci.9b00184
ACS Cent. Sci. 2019, 5, 1017−1023

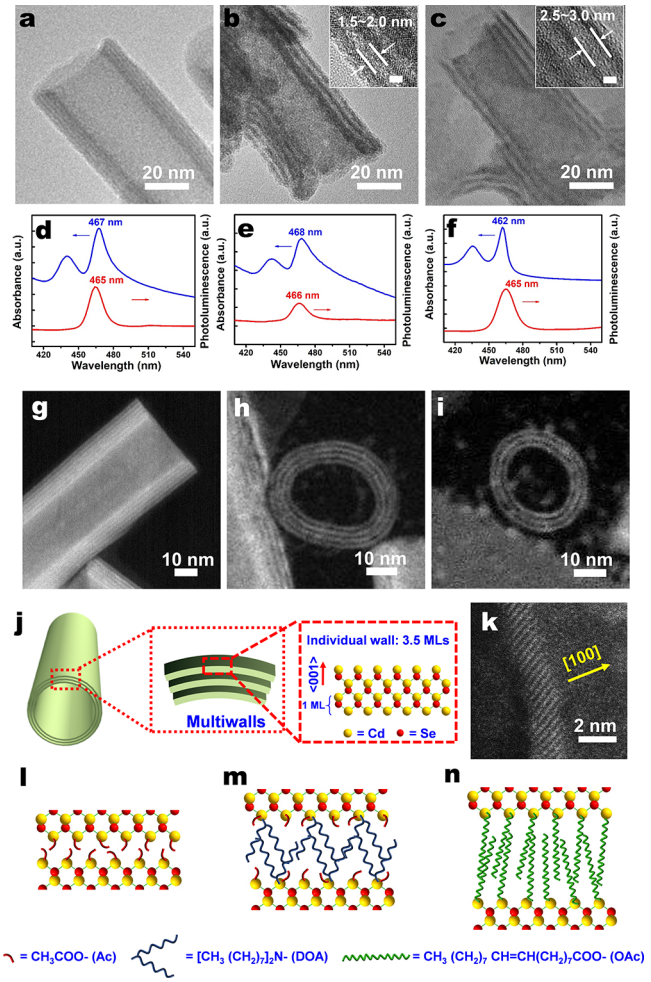

Figure 2. Multiwalled character of the CdSe NTs, as observed by TEM, STEM, PL, and UV–vis absorption spectroscopy. TEM micrographs of CdSe NTs, synthesized from Cd acetate-dioctylamine ($Cd(Ac)_2$-DOA) and Se-octadecene (Se-ODE) precursor solutions at 260 °C during a reaction time of (a) 8 min, (b) 256 min, and (c) 8 min, with the additional exchange of Ac ligands by oleic acid (OAc) at 200 °C in part c. (d–f) UV–vis absorbance and PL spectra of a solution in hexane of CdSe NTs corresponding to the structures of parts a–c, respectively. The major absorbance and PL peaks are indicative of a quasi-2D CdSe nanostructure with an individual wall thickness of 3.5 MLs. HAADF-STEM graphs of a CdSe NTs synthesized within 8 min at 260 °C when observed along the (g) tube-side direction and (h, i) tube-opening direction. (j) Schematic illustration of a multiwalled CdSe NT. (k) HAADF-STEM graph of an individual wall consisting of 3.5 MLs with ⟨100⟩ normal direction. (l–n) Schematic illustrations of the CdSe NTs corresponding to the structures of parts a–c, showing how the use of different ligands leads to different spacings between individual walls.

with a longer-chain ligand. This idea was first verified by extending the synthesis time to 256 min. These samples, even though they have quite similar absorption and emission spectra as those synthesized within 8 min (Figure 2e), present an obvious multiwalled structure under TEM (Figure 2b). Apparently, even though DOA is a weaker ligand compared to carboxylate,[23] it is capable of intercalating the walls in the presence of acetate ligand, when exposed over a long time in a nonpolar environment. The FTIR spectrum confirms the dominant role of DOA by a huge increase of the characteristic peaks of DOA (Figure S4). According to the Tanford formula,[26] the maximum extensional length of an 8 carbon chain is 1.17 nm. The measured spacing between walls is 1.5–2.0 nm, indicating a small interpenetration between two face-to-face alkylamines (Figure 2m). The XRD measurement of the sample prepared at 260 °C for 256 min (Figure S3) displays a high-angle shift of the whole pattern over about 1°, which can be due to surface-related effects that affect the overall sample structure and effective lattice constant.[27] Finally, we performed ligand exchange of the CdSe NTs synthesized within 8 min with oleic acid at 200 °C for 10 min (Figure 2c). Remarkably, most of NT aggregates are disintegrated and exfoliated into sheetlike nanostructures with more uniform and separate walls (Figure S8). The first excitonic peak shifts to 462 nm (Figure 2f), close to that of flat nanoplatelets. Some partly broken NTs of Figure 2c maintain the stacking arrangement of multiple walls, exhibiting a spacing of 2.5–3.0 nm between walls, which is less than the maximum extensional length of 4.86 nm between two face-to-face oleic acids, as calculated according to the Tanford formula (Figure 2c,n). These two cases convincingly demonstrate the multiwalled character of NTs. On the basis of the HAADF-STEM analysis (Figure S8c,d, Figure 2k), the thickness of the NCs was determined to be around 1.5 nm. In the literature, an individual wall is considered to be composed of 3.5 MLs, i.e., 4 Cd layers and 3 Se layers alternating along the ⟨001⟩ normal direction.[10,27]

Role of the Amine and Acetate Ligands in CdSe NT Synthesis. To understand the formation of the CdSe NTs, the role of DOA was first investigated. We noticed the occurrence of white precipitates, once the clear $Cd(Ac)_2$-DOA solution was injected into the hot Se-ODE solution. In a control experiment, we replaced the Se-ODE solution with a Se-DOA solution, and doing so, no precipitates appeared immediately after injecting Cd precursor; however, a dark solution was obtained for a reaction time of 8 min. The TEM graph of Figure S9b shows the assembly of CdSe nanodots into mesocrystals[28] instead of CdSe NTs. Moreover, no peak is found in the UV–vis absorption spectra, suggesting no quantum confinement behavior for these nanoscale assemblies (Figure S9g). Hence, ODE seems important, and our experiments suggest that the precipitates play a role in the formation of the NTs. For further characterization, we therefore separated the precipitates in a pure hot ODE solution, which we label as $Cd(Ac)_2$-DOA precipitates. Unexpectedly, FTIR spectra demonstrated that the latter had a strong signal originating from COO– bonds and a negligible signal due to C–H bonds, similar to the spectra of $Cd(Ac)_2\cdot 2H_2O$ powder but quite different from those of the $Cd(Ac)_2$-DOA precursor solution (Figure S10). Moreover, analysis based on TEM (Figure S11a,b), SAED (Figure S11c), HRTEM (Figure S11d–f), and XRD (Figure S12a) demonstrated that their morphology is almost identical to $Cd(Ac)_2\cdot 2H_2O$ powder, showing cadmium oxide (CdO) NCs less than 10 nm in diameter and uniformly dispersed in an amorphous matrix. These results therefore suggest that the $Cd(Ac)_2$-DOA precipitates are essentially due to the precipitation of $Cd(Ac)_2$ in ODE solvent (hydrate water is removed because of the elevated temperature). This triggered the question of whether 2D CdSe NCs could be obtained solely from $Cd(Ac)_2\cdot 2H_2O$ and Se powder precursors, without using DOA.

We therefore reacted the mixture of $Cd(Ac)_2\cdot 2H_2O$ and Se powder in ODE at 260 °C. As shown in Figure S9c,g,h, a sample prepared within 8 min shows ill-defined multiwalled

DOI: 10.1021/acscentsci.9b00184
ACS Cent. Sci. 2019, 5, 1017–1023

NTs with both lateral and angular extension, and their 2D electronic structure is verified by the sharp absorption at 467 nm and emission at 464 nm. Compared with the NTs prepared in the presence of DOA, intact tubular architectures were difficult to find. We hypothesized that this is because of the insufficient mass transfer between $Cd(Ac)_2{\cdot}2H_2O$ and Se powder, given that both solid ingredients have low solubility in ODE. Increasing the reaction time to 16 min, ultrathin and sheetlike nanostructures were observed in the presence of numerous irregular nanodots (Figure S9d). For products synthesized within 32 min (Figure S9e), we see broken sheetlike nanostructures together with an increasing number of nanodots. Their absorption peak exhibits a blue shift to 462 nm, suggesting less interwall coupling. In brief, these experiments indicate the generation of ill-defined tubelike nanostructures, which gradually decompose into ultrathin sheetlike nanostructures and eventually into irregular nanodots, as the reaction evolves. A possible explanation is that, because of the fast reaction between Cd and Se precursors in the asbence of DOA ligand, the CdSe monomer concentration is rapidly consumed to a low level, leading to Ostwald ripening of the nanodots at the expense of tubelike nanostructures.

To test the role of the ODE solvent, we simply heated the mixture of $Cd(Ac)_2{\cdot}2H_2O$ and Se powders at 260 °C in air without the use of ODE. A previous report showed the formation of CdSe nanoplatelets by reacting $Cd(propionate)_2$ or $Cd(myristate)_2$ with Se powder at 200 °C.[16] Surprisingly, in our experiments, multiwalled CdSe NTs were also found, showing characteristic absorption and PL peaks of 2D CdSe NCs around 460 and 510 nm (Figure S9f–h), together with some unreacted Cd precursor. This could be ascribed to the high insolubility caused by the acetate ligand and high energy required for the assembly of the nanotubes. These investigations suggest that the anisotropic growth of the 2D CdSe NCs essentially originates from the acetate ligand that can passivate the growth of {100} planes of zincblende CdSe NCs in a solid (or partly melted) Cd precursor matrix, while the amine just plays an auxiliary role by regulating the reaction process and improving the mass transfer between Cd and Se precursors. We also investigated the influence of other alkylamines by replacing DOA with primary amines like octylamine (OAm) and oleylamine (OLA) and a tertiary amine like trioctylamine (TOA). Due to the steric effect, the solubility of $Cd(Ac)_2$ in different alkylamines would be as follows: the primary amine allows better solubility than the secondary amine, and the secondary amine allows better solubility than the tertiary amine. As shown in Figure S13, if the solubility is good, we obtained CdSe nanobelts (Figure S13d) and irregular CdSe nanoparticle aggregates (Figure S13f) when using $Cd(Ac)_2$-OAm and $Cd(Ac)_2$-OLA as the precursor, respectively. If the solubility is bad, less well-defined tubular-like CdSe nanocrystals were prepared, corresponding to the case of using $Cd(Ac)_2$-TOA as the precursor (Figure S13e). These results, together with the data of Figure 1, suggest that DOA offers great advantages for producing better defined tubular structures.

CdSe NTs Growth Mechanism. To further elucidate the growth mechanism when using the $Cd(Ac)_2$-DOA solution as the Cd precursor, we performed a series of experiments to trace the evolution of the tubular structure by tailoring the reaction time at different temperatures, i.e., at 80, 140, 200, and 260 °C. All the samples exhibit characteristic absorption and emission spectra of 2D CdSe NCs with the first excitonic peak around 390 or 460 nm, depending on the synthetic temperature. The good continuity provided by the microscopic and spectroscopic results (Figures S14–S17) clearly demonstrates the anisotropic growth of the CdSe NTs by a nonplanar 2D-oriented attachment approach, in which three critical stages are observable: formation of nanoplatelets, curved nanosheets, and tubular NCs.

In the first stage, anisotropic nanoplatelets with a thickness of 1–2 nm and length of 3–5 nm were found in samples prepared at 80 °C within 17 h (Figure S14) and 140 °C within 8 min (Figure 3b,c, Figure S15a). Apart from the sharp peak at around 390 nm, their emission spectra also show a rather broad peak around 480 nm, which could be ascribed to a deep trap-state emission.[15] Figure S18 reveals the formation of these anisotropic seeds by heterogeneous nucleation from the amorphous Cd precursor matrix. This nucleation mode has a greatly reduced energy barrier, rapidly resulting in a large number of nuclei in a highly concentrated environment. The use of short-chain acetate plays an important role, since it provides a low solubility of ligand-capped monomers in the nonpolar solvent. Also, because of the low steric hindrance of the acetate ligand, the formed CdSe nuclei are highly reactive, ready for the further attachment with the adjacent ones. In terms of packing density and dangling bonds, the passivated surface energies of zincblende CdSe have the following relation: $\gamma_{\{100\}} < \gamma_{\{111\}} < \gamma_{\{110\}}$.[29] Therefore, the growth is hindered along the polar ⟨100⟩ direction while it is favored along the nonpolar ⟨110⟩ direction, giving rise to nanoplatelets with two polar {100} planes at both the top and bottom surface.

In the second stage, the nanoplatelets are assembled into a curved nanosheet by simultaneously lateral and angular attachment. Lateral attachment, such as that occurring for ultrathin PbS nanosheets,[30] takes place on the most reactive {110} facets of two adjacent nanoplatelets (Figure 3d, Figure S14b): the process involves alignment, contact, fusion, and a post-recrystallization process to eliminate the crystal boundary.[31] The patchlike structure of Figure 3e provides evidence of growth by oriented attachment rather than by monomer addition.[30] However, due to the low orientational degree of freedom inside the solid Cd precursor matrix, the alignment and rotation of the building blocks are severely constrained. As a result, growth via angular attachment is more prevalent. Two main types of assembly contributing to the angular growth are observed: misoriented attachment and multiple oriented attachment. The former involves relatively small angular rotations (<24°) between two neighboring {110} facets, resulting in crystal defects that include stacking faults (Figure 4a), lattice distortions (Figure 4b), and edge dislocations (Figure 4c,d). These defects are characteristic features of nanostructures formed via oriented attachment.[28,31] The latter can take place on a less reactive {111} facet through attachment with a {110} facet (Figure 4e) or via attachment of two {111} facets (Figure 4f), resulting in a large misoriented angle of 35° and 70°, respectively. The presence of a high number of crystal defects is expected, whereby the requirement of a large asymmetric strain on both sides of the tube wall can be satisfied.

In the final stage, well-defined CdSe NTs are obtained via assembly of the curved nanosheets. This is clearly demonstrated by the arrangement of curved nanosheets into early stage tubelike architectures within 0.5 min at 260 °C (Figure S17a). By forming a tubular morphology, the reactive {110}

DOI: 10.1021/acscentsci.9b00184
ACS Cent. Sci. 2019, 5, 1017–1023

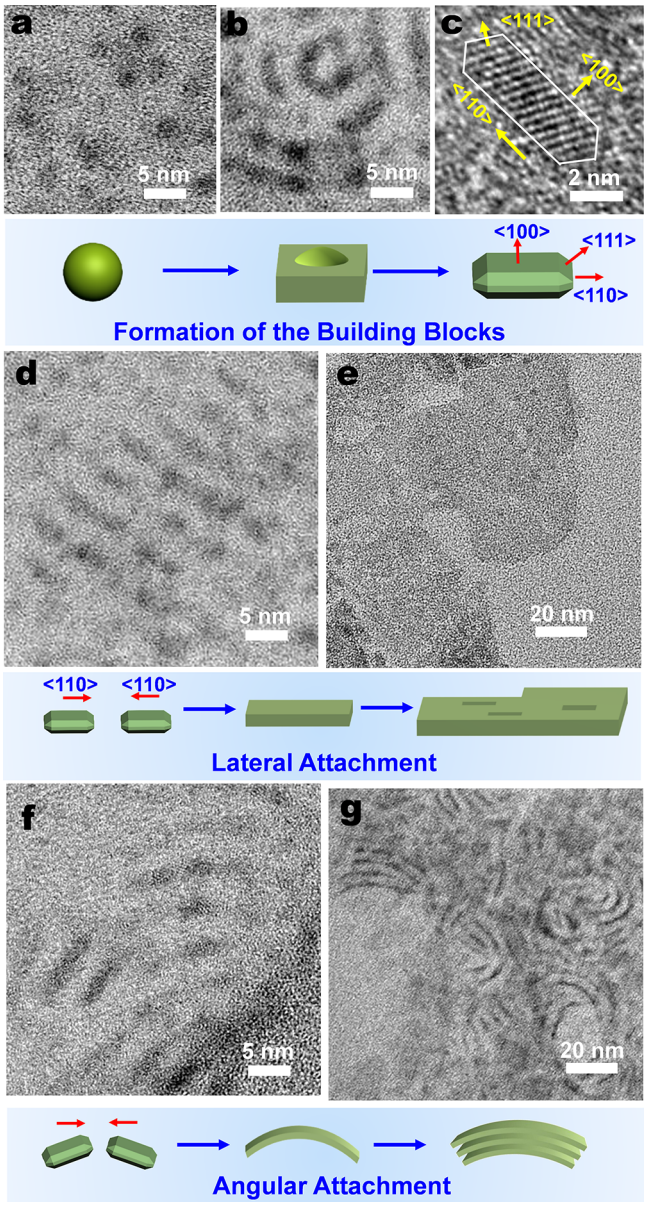

Figure 3. TEM and HRTEM study of early formation stages of CdSe NTs. (a–d, f) Synthesis at a temperature of 140 °C leads to (a) CdSe dots of around 2 nm as well as (b) seeds that form NT building blocks in the form of elongated platelets. (c) HRTEM micrograph of a small assembly of building blocks showing lattice fringe of {111} facets. The schematic shows the formation of building blocks from the CdSe dots to platelets with {100} terrace facets. (d) Lateral growth mechanism, as indicated by the attachment of the building blocks in the ⟨110⟩ direction. (e) Synthesis at a temperature of 200 °C allows the observation of holes in the nanosheets, indicative of a growth mechanism by building block assembly. (f) Angular growth mechanism by the assembly of building blocks with a rotation with respect to the ⟨110⟩ direction. (g) Formation of initial multiwalled structures as result of the angular growth mechanism and intermolecular forces between individual walls.

surfaces can be thus eliminated. Due to the high strain energy in a tubular nanostructure,[32] both intact and incomplete assemblies are easily observed in the samples synthesized within 8 min (Figure S19). It is noticeable that NTs are only found when the reaction temperature is above 200 °C, while samples prepared at 80 and 140 °C just show nanoplatelets

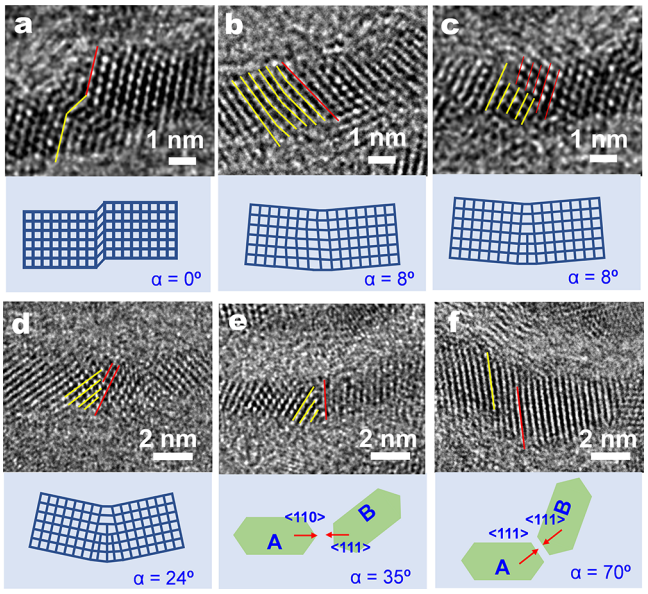

Figure 4. HRTEM study of the angular assembly mechanism. (a) HRTEM image of a distorted lattice plane due to a stacking fault along the ⟨111⟩ direction, not resulting in a microscopic rotation of the crystallographic orientation ($\alpha = 0°$). (b) A small angular rotation ($\alpha = 8°$) is caused by a lattice distortion on the {111} facets. Edge dislocations involving (c) one or (d) three half atomic planes into the {111} facts are also observed, contributing to an angular rotation of 8° and 24°, respectively. The oriented attachment between (e) {110} and {111} planes as well as (f) two adjacent {111} planes leads to a larger angular rotation of 35° and 70°, respectively. The red and yellow lines indicate the {111} facets in adjacent building blocks.

(Figure S14) and curved nanosheets (Figure S15), respectively. This means that the nucleation energy barrier is lower than the required energy for growth by attachment. We think that the formation of well-defined tubular structures requires a balance between lateral and angular growth. Raising the temperature even higher would provide more energy to overcome the barrier of oriented attachment and, more importantly, facilitate the lateral attachment by enhancing the motion of building blocks in the precursor matrix.

To check if these tubular nanostructures are similar to the nanoscrolls often found during growth of CdSe nanosheets with a large lateral dimension,[9,10] an unfolding process by growing a CdS shell on the CdSe NT was performed. The CdSe NTs, synthesized at 260 °C within 8 min, were first reacted with a thiol ligand, thioacetamide (TTA), followed by the addition of a $Cd(oleate)_2$ precursor. As shown in Figure S20, we find fragmented nanosheets with lateral dimension less than 200 nm in our NTs after the treatment, which is different from the large rectangular nanosheets observed when unfolding nanoscrolls.[9,10] Further investigation allowed the determination that these sheetlike fragments already existed after reacting the NTs with TTA (Figure S21). This result is expected, as surface ligand exchange would diminish the interwall interaction formed by the acetate ligand, thus disintegrating tubular nanostructures into sheetlike fragments in the presence of crystal defects.

A striking property of the CdSe NTs is their ability to catalyze a redox reaction under visible-light irradiation. Figure 5 presents the rapid photocatalytic reduction of Rhodamine B (RhB) into its leuco form when NTs are used as catalysts, reaching a conversion rate of 92% in 1 min. The photocatalytic

DOI: 10.1021/acscentsci.9b00184
ACS Cent. Sci. 2019, 5, 1017–1023

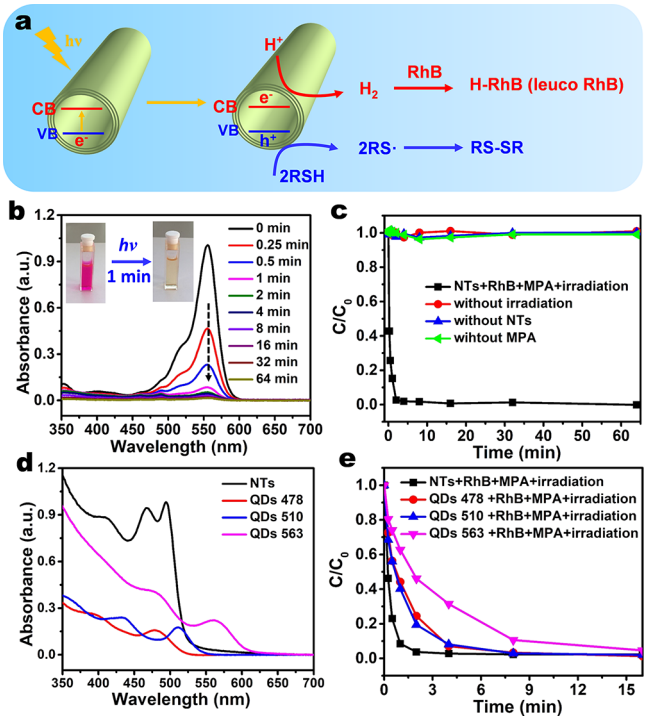

Figure 5. Visible-light photocatalytic reduction of RhB into its leuco form by using the CdSe NTs as photocatalysts. (a) Schematic illustration of the photoreduction of aqueous Rhodamine B (RhB). Under visible-light irradiation, CdSe NTs have holes in the valence band (VB) and electrons in the conduction band (CB). The former can oxidize thiols into thiolate radicals, which finally turn into more stable disulfides; the latter can reduce the protons into hydrogen, which further react with RhB to produce its leuco form. (b) Photoreduction of the RhB in the presence of CdSe NTs and 3-mercaptopropionic acid (MPA) at different light irradiation time. The inset shows the rapid decolorization of RhB after irradiation for 1 min. (c) Temporal evolution of the concentration of RhB in the presence of the NTs, MPA, and light irradiation. Control experiments in the absence of NTs, MPA, or light irradiation are also shown. (d) Absorption spectra of as-synthesized CdSe NTs and three quantum dots (QDs 478, QDs 510, and QDs 563) samples in water. The concentrations are all 0.104 mg/mL. (e) Temporal evolution of the RhB concentration during the photoreduction using CdSe NTs, QDs 478, QDs 533, and QDs 563 as the photocatalysts. The concentrations of the catalysts are all 0.05 mg/mL.

process is depicted in Figure 5a: under light irradiation, the valence electrons in the NTs are excited to the conduction band (CB), leaving holes with high potential in the valence band (VB). Water-soluble thiols (RSH) are thereby rapidly oxidized into sulfur-center radicals and more stable disulfides by the holes.[33] To realize this photocatalytic reaction, the NTs were first transferred into water by surface ligand exchange with 3-mercaptopropionic acid (MPA). A red-shift of about 30 nm of the first absorption peak was observed when the NTs were well-dispersed in water (Figure 5d). After purification, the NTs and an additional 5 μL of MPA were added to the aqueous RhB solution, followed by light irradiation from a halogen lamp to trigger the reaction. Control experiments demonstrated that the use of NTs, MPA, and light irradiation is all necessary, the absence of one of them resulting in no change in the RhB signal (Figure 5c, Figure S22a–c). The intrinsic high affinity of the MPA to the NTs plays an important role in inhibiting the combination of the holes with electrons. Meanwhile, protons in the water are reduced into hydrogen by grabbing the electrons from the NTs, which further react with the RhB to form colorless RhB (Scheme S1 of the Supporting Information).[34,35] In the presence of oxygen, leuco RhB could recover to the normal form, showing a recovery rate of 39% after 30 h (Figure S23). This means that the chromophore groups were not irreversibly destroyed during the photoreduction.[36]

To further evaluate the photocatalytic activity of the NTs, three CdSe quantum dots (QDs) samples, marked as QDs 478, QDs 510, and QDs 563 according to their respective first excitonic peaks, were synthesized for comparison (Figure S24). Absorption spectra of the NTs and QDs at the same concentration in water demonstrate that the NTs have much stronger absorption than the QDs (Figure 5d). Figure 5e reveals that it takes 4, 4, and 8 min for the reaction to reach a conversion rate above 90% in the presence of QDs 478, QDs 510, and QDs 563 as the catalysts, respectively (Figure 5e, Figure S22d–f), all of which are longer than in the case of NTs. The improved photocatalytic activity by the NTs is mainly ascribed to (1) a larger band gap when compared with the QDs 563 or (2) a larger absorption cross-section when compared with QDs 478 and QDs 510. TEM and STEM imaging demonstrated maintenance of a tubelike morphology after a photoreaction reaction of 30 min (Figure S25).

Safety Statement. No unexpected or unusually high safety hazards were encountered.

CONCLUSIONS

In conclusion, we have demonstrated a template-free pathway to synthesize zincblende CdSe NTs with atomically flat walls. They feature a multiwalled structure, sharp absorption and emission at around 460 nm, and Cd-terminated {100} planes as the top and bottom surface in the wall thickness direction. Anisotropic growth is found to result from the utilization of acetate ligand; meanwhile, the addition of DOA assists in the formation of more regular tubular structures. We further elucidated that the growth mechanism is a nonplanar 2D oriented attachment approach, that is, the simultaneous lateral and angular attachment of early stage 2D nanoplatelets into curved nanosheets and finally into a tubular architecture. Remarkably, they present highly efficient photocatalysis reactivity under visible light due to the suitable band gap and large absorption cross-section. It is envisioned that this work will shed new light on the understanding of 2D CdSe NCs formation and the synthesis of other complex anisotropic nanostructures.

ASSOCIATED CONTENT

Supporting Information

The Supporting Information is available free of charge on the ACS Publications website at DOI: 10.1021/acscentsci.9b00184.

Experimental details, detailed STEM, UV–vis, PL, XRD characterization, FTIR spectra, and TEM graphs (PDF)

AUTHOR INFORMATION

Corresponding Author

*E-mail: martin.gijs@epfl.ch.

ORCID

Xiaopeng Huang: 0000-0002-4882-9331

Virendra K. Parashar: 0000-0003-2082-1028

DOI: 10.1021/acscentsci.9b00184
ACS Cent. Sci. 2019, 5, 1017–1023

Funding

This work was financially supported by the Swiss National Science Foundation (Grant 200021-146237) and China Scholarship Council (201406360047).

Notes

The authors declare no competing financial interest.

■ ACKNOWLEDGMENTS

The Centre Interdépartemental de Microscopie Electronique (CIME) at EPFL is acknowledged for providing the access and training to SEM and TEM facilities. We thank Dr. Thomas LaGrange and Lichen Bo for the help in the STEM imaging using Titan Themis.

■ REFERENCES

(1) Peng, X.; Manna, L.; Yang, W.; Wickham, J.; Scher, E.; Kadavanich, A.; Alivisatos, A. P. Shape control of CdSe nanocrystals. *Nature* **2000**, *404* (6773), 59.

(2) Manna, L.; Milliron, D. J.; Meisel, A.; Scher, E. C.; Alivisatos, A. P. Controlled growth of tetrapod-branched inorganic nanocrystals. *Nat. Mater.* **2003**, *2* (6), 382−385.

(3) Joo, J.; Son, J. S.; Kwon, S. G.; Yu, J. H.; Hyeon, T. Low-temperature solution-phase synthesis of quantum well structured CdSe nanoribbons. *J. Am. Chem. Soc.* **2006**, *128* (17), 5632−5633.

(4) Ithurria, S.; Dubertret, B. Quasi 2D colloidal CdSe platelets with thicknesses controlled at the atomic level. *J. Am. Chem. Soc.* **2008**, *130* (49), 16504−16505.

(5) Ithurria, S.; Tessier, M. D.; Mahler, B.; Lobo, R. P.; Dubertret, B.; Efros, A. L. Colloidal nanoplatelets with two-dimensional electronic structure. *Nat. Mater.* **2011**, *10* (12), 936−941.

(6) Li, Z.; Peng, X. Size/shape-controlled synthesis of colloidal CdSe quantum disks: ligand and temperature effects. *J. Am. Chem. Soc.* **2011**, *133* (17), 6578−6586.

(7) Son, J. S.; Wen, X. D.; Joo, J.; Chae, J.; Baek, S. I.; Park, K.; Kim, J. H.; An, K.; Yu, J. H.; Kwon, S. G.; Choi, S. H.; Wang, Z.; Kim, Y. W.; Kuk, Y.; Hoffmann, R.; Hyeon, T. Large-scale soft colloidal template synthesis of 1.4 nm thick CdSe nanosheets. *Angew. Chem., Int. Ed.* **2009**, *48* (37), 6861−6864.

(8) Liu, Y. H.; Wang, F.; Wang, Y.; Gibbons, P. C.; Buhro, W. E. Lamellar assembly of cadmium selenide nanoclusters into quantum belts. *J. Am. Chem. Soc.* **2011**, *133* (42), 17005−17013.

(9) Bouet, C.; Mahler, B.; Nadal, B.; Abecassis, B.; Tessier, M. D.; Ithurria, S.; Xu, X.; Dubertret, B. Two-dimensional growth of CdSe nanocrystals, from nanoplatelets to nanosheets. *Chem. Mater.* **2013**, *25* (4), 639−645.

(10) Mahler, B.; Nadal, B.; Bouet, C.; Patriarche, G.; Dubertret, B. Core/shell colloidal semiconductor nanoplatelets. *J. Am. Chem. Soc.* **2012**, *134* (45), 18591−18598.

(11) Son, J. S.; Yu, J. H.; Kwon, S. G.; Lee, J.; Joo, J.; Hyeon, T. Colloidal synthesis of ultrathin two-dimensional semiconductor nanocrystals. *Adv. Mater.* **2011**, *23* (28), 3214−3219.

(12) Bouet, C.; Tessier, M. D.; Ithurria, S.; Mahler, B.; Nadal, B.; Dubertret, B. Flat colloidal semiconductor nanoplatelets. *Chem. Mater.* **2013**, *25* (8), 1262−1271.

(13) Wang, F.; Wang, Y.; Liu, Y. H.; Morrison, P. J.; Loomis, R. A.; Buhro, W. E. Two-dimensional semiconductor nanocrystals: properties, templated formation, and magic-size nanocluster intermediates. *Acc. Chem. Res.* **2015**, *48* (1), 13−21.

(14) Nasilowski, M.; Mahler, B.; Lhuillier, E.; Ithurria, S.; Dubertret, B. Two-dimensional colloidal nanocrystals. *Chem. Rev.* **2016**, *116* (18), 10934−10982.

(15) Ithurria, S.; Bousquet, G.; Dubertret, B. Continuous transition from 3D to 1D confinement observed during the formation of CdSe nanoplatelets. *J. Am. Chem. Soc.* **2011**, *133* (9), 3070−7.

(16) Riedinger, A.; Ott, F. D.; Mule, A.; Mazzotti, S.; Knusel, P. N.; Kress, S. J. P.; Prins, F.; Erwin, S. C.; Norris, D. J. An intrinsic growth instability in isotropic materials leads to quasi-two-dimensional nanoplatelets. *Nat. Mater.* **2017**, *16* (7), 743−748.

(17) Chen, Y.; Chen, D.; Li, Z.; Peng, X. Symmetry-breaking for formation of rectangular CdSe two-dimensional nanocrystals in zinc-blende structure. *J. Am. Chem. Soc.* **2017**, *139* (29), 10009−10019.

(18) Iijima, S. Helical microtubules of graphitic carbon. *Nature* **1991**, *354* (6348), 56.

(19) Yu, D.; Liu, F. Synthesis of carbon nanotubes by rolling up patterned graphene nanoribbons using selective atomic adsorption. *Nano Lett.* **2007**, *7* (10), 3046−3050.

(20) Zhou, M.; Zhu, H.; Wang, X.; Xu, Y.; Tao, Y.; Hark, S.; Xiao, X.; Li, Q. CdSe nanotube arrays on ITO via aligned ZnO nanorods templating. *Chem. Mater.* **2010**, *22* (1), 64−69.

(21) Kim, J. W.; Shim, H.-S.; Ko, S.; Jeong, U.; Lee, C.-L.; Kim, W. B. Thorny CdSe nanotubes via an aqueous anion exchange reaction process and their photoelectrochemical applications. *J. Mater. Chem.* **2012**, *22* (39), 20889−20895.

(22) Boles, M. A.; Ling, D.; Hyeon, T.; Talapin, D. V. The surface science of nanocrystals. *Nat. Mater.* **2016**, *15* (3), 141−153.

(23) Chen, P. E.; Anderson, N. C.; Norman, Z. M.; Owen, J. S. Tight binding of carboxylate, phosphonate, and carbamate anions to stoichiometric CdSe nanocrystals. *J. Am. Chem. Soc.* **2017**, *139* (8), 3227−3236.

(24) Wu, Z.; Liu, J.; Li, Y.; Cheng, Z.; Li, T.; Zhang, H.; Lu, Z.; Yang, B. Self-assembly of nanoclusters into mono-, few-, and multilayered sheets via dipole-induced asymmetric van der waals attraction. *ACS Nano* **2015**, *9* (6), 6315−6323.

(25) Cho, K.-S.; Talapin, D. V.; Gaschler, W.; Murray, C. B. Designing PbSe nanowires and nanorings through oriented attachment of nanoparticles. *J. Am. Chem. Soc.* **2005**, *127* (19), 7140−7147.

(26) Tanford, C. Micelle shape and size. *J. Phys. Chem.* **1972**, *76* (21), 3020−3024.

(27) Chen, D.; Gao, Y.; Chen, Y.; Ren, Y.; Peng, X. Structure identification of two-dimensional colloidal semiconductor nanocrystals with atomic flat basal planes. *Nano Lett.* **2015**, *15* (7), 4477−4482.

(28) Colfen, H.; Antonietti, M. Mesocrystals: inorganic superstructures made by highly parallel crystallization and controlled alignment. *Angew. Chem., Int. Ed.* **2005**, *44* (35), 5576−5591.

(29) Debnath, S.; Cherian, R.; Mahadevan, P. The role of passivants on the stoichiometry of CdSe and GaAs nanocrystals. *J. Phys. Chem. C* **2013**, *117*, 21981−21987.

(30) Schliehe, C.; Juarez, B. H.; Pelletier, M.; Jander, S.; Greshnykh, D.; Nagel, M.; Meyer, A.; Foerster, S.; Kornowski, A.; Klinke, C. Ultrathin PbS sheets by two-dimensional oriented attachment. *Science* **2010**, *329* (5991), 550−553.

(31) Penn, R. L.; Banfield, J. F. Imperfect oriented attachment: dislocation generation in defect-free nanocrystals. *Science* **1998**, *281* (5379), 969−971.

(32) Remškar, M. Inorganic nanotubes. *Adv. Mater.* **2004**, *16* (17), 1497−1504.

(33) Li, X.-B.; Li, Z.-J.; Gao, Y.-J.; Meng, Q.-Y.; Yu, S.; Weiss, R. G.; Tung, C.-H.; Wu, L.-Z. Mechanistic insights into the interface-directed transformation of thiols into disulfides and molecular hydrogen by visible-jight irradiation of quantum dots. *Angew. Chem., Int. Ed.* **2014**, *53* (8), 2085−2089.

(34) Li, Y.; Lu, G.; Li, S. Photocatalytic transformation of rhodamine B and its effect on hydrogen evolution over Pt/TiO_2 in the presence of electron donors. *J. Photochem. Photobiol., A* **2002**, *152* (1−3), 219−228.

(35) Zhao, J.; Holmes, M. A.; Osterloh, F. E. Quantum confinement controls photocatalysis: a free energy analysis for photocatalytic proton reduction at CdSe nanocrystals. *ACS Nano* **2013**, *7* (5), 4316−4325.

(36) Wang, W.; Ye, M.; He, L.; Yin, Y. Nanocrystalline TiO_2-catalyzed photoreversible color switching. *Nano Lett.* **2014**, *14* (3), 1681−1686.

DOI: 10.1021/acscentsci.9b00184
ACS Cent. Sci. 2019, 5, 1017−1023